Real-Time X-ray Diffraction Study on Two-Stage Drawing of Ultra-High Molecular Weight Polyethylene Reactor Powder above the Static Melting Temperature

Hiroki Uehara and Tetsuo Kanamoto*

Department of Applied Chemistry, Science University of Tokyo, Kagurazaka, Shinjuku-ku, Tokyo 162, Japan

Akiyoshi Kawaguchi and Syozo Murakami

The Institute of Chemical Research, Kyoto University, Uji, Kyoto 611, Japan

Received August 21, 1995; Revised Manuscript Received November 14, 1995[⊗]

ABSTRACT: The polyethylene for the study was ultra-high molecular weight polyethylene (UHMW-PE) reactor powder extrusion drawn to a low draw ratio (DR) of ∼6 (first-stage draw). The structural change during the second-stage tensile draw of the extrudate has been studied above the static melting point by real-time wide-angle X-ray diffraction (WAXD). Information on the phase structure was also obtained by WAXD as a function of sample DR, temperature (T_d), and applied tensile load and by retractive stress measurements. Upon heating the extrudate with the fixed ends in an X-ray high-temperature chamber, part of the initially orthorhombic crystals transformed into the hexagonal crystalline and amorphous phases at ≥150 °C, indicating that the retractive stress was not homogeneously distributed within a drawn sample. Such a transformation temperature increased with sample DR. When draw was initiated at a constant T_d of 150−155 °C, the chain orientation in both the hexagonal and the amorphous phases rapidly increased, and these phases transformed into the orthorhombic crystals. Even when the T_d was raised to 160 °C during drawing, the orthorhombic phase was predominant with no significant increase in the amorphous component. These results show that the major deformation proceeded in a highly crystalline state where the orthorhombic crystalline phase was predominant, giving an efficient draw in terms of molecular DR, at least up to 155 °C, and reflecting the characteristics of the UHMW-PE reactor powder used in this work. Such deformation behavior in the high-temperature range is markedly different from that previously reported for single-crystal mats and gel and melt-crystallized films of UHMW-PE, which produced poor mechanical properties.

Introduction

In previous papers,[1,2] we have shown that films prepared by the compaction of ultra-high molecular weight polyethylene (UHMW-PE) reactor powder, below the static melting point, are too brittle to be drawn by straight tensile drawing. However, they became highly ductile after solid-state coextrusion at a low extrusion draw ratio (EDR) of ∼6 (first-stage draw). The extruded films could be effectively drawn in a crystalline state at ∼135 °C to DR ≤ 85 by tensile force (second-stage draw).[1] Such highly drawn films, prepared by the two-stage draw, exhibited tensile moduli ≤145 GPa and strength ≤1.8 GPa at room temperature. Further, the optimum T_d for the second-stage tensile drawing strongly depends on the catalyst used, polymerization conditions, and the molecular weight of UHMW-PE reactor powders.[3,4] It was also found that the optimum T_d for some samples was 145−155 °C, which is significantly above the static melting temperature, ∼140 °C, of UHMW-PE reactor powder.[4] Thus, in this work, the structural changes in compacted films of UHMW-PE reactor powders extrusion drawn to an EDR of ∼6 have been studied during the second-stage drawing at 145−160 °C, above their static melting point. The phase transformation from the orthorhombic to the hexagonal phase and to the melt during deformation will be emphasized. The effects of applied tension and sample DR on the phase transition will also be discussed.

The usual orthorhombic phase of PE transforms into the hexagonal phase above 150 °C, as observed for UHMW-PE surface-grown fibers[5] and highly drawn gel fibers[6,7] heated at a constant length. This phase is also known to occur at high temperatures and pressures.[8,9] Raman spectroscopy[10] and X-ray diffraction[11] results indicate that this phase contains a significant fraction of gauche conformers. This phase is also called a "rotator phase", since the molecular chains rapidly rotate around the chain axis and the chains easily slide past each other. In the hexagonal phase, thus, the applied stress rapidly relaxes leading to the melt, as was observed upon heating of the oriented UHMW-PE fibers[5,7] with the fixed sample ends. Upon drawing of gel[6] and melt-crystallized films[12] of UHMW-PE at T_d > 135 °C, the efficiency of draw was low in terms of molecular draw ratio (MDR)[13] since once the orthorhombic phase transformed completely to the melt or partly to the hexagonal, the applied stress could not be effectively transmitted within a sample. Similar behavior was also observed upon tensile drawing of poly(*trans*-1,4-butadiene) in the rotator phase.[14]

Experimental Section

Drawing. The two UHMW-PE reactor powders used in this work were polymerized by a high-activity Ziegler catalyst at 40 °C. They had M_v's of 1.8 and 5.3 × 10^6. These powders were compression molded into films at 130 ± 0.5 °C, which is ∼10 °C below the DSC melting peak temperatures, and 12 MPa for 30 min. A strip (3 × 0.3 × 50 mm) cut out from the compacted powder film was sandwiched between split billet halves of high-density polyethylene, and the assembly was coextruded at 125 °C and a low EDR of ∼6. For the second-stage drawing, the extrudate was drawn by tensile force at constant T_d's of 135−160 °C and at constant cross-head speeds, giving an initial strain rate of 0.7−2 min^{-1} on a Tensilon tensile tester RTM-100 equipped with an air oven or in a high-

[⊗] Abstract published in *Advance ACS Abstracts,* February 1, 1996.

0024-9297/96/2229-1540$12.00/0

temperature X-ray diffraction chamber. The true draw stress was calculated by the nominal stress divided by the cross-sectional area of a sample at a given strain. The total DR (DR_t) was defined by DR_t = (initial EDR) × (second-stage tensile DR). The accuracy of the temperature was ±0.5 °C in most of the experiments.

Measurements. Wide-angle X-ray diffraction (WAXD) patterns of drawn UHMW-PE reactor powder films at elevated temperatures were measured (1) at a constant length, (2) at a constant load, and (3) during drawing at constant temperatures ≤160 °C. These patterns were recorded by using (1) a conventional Rigaku diffractometer combined with a fiber specimen holder equipped with a temperature controller or (2) MAC-Science Type DIP220 imaging plates combined with a high-temperature drawing device, whose details are reported elsewhere.[15] Cu Kα radiation monochromatized with a Ni filter or graphite monochrometer was generated at 40 kV and 150−240 mA by a Rigaku Type RU-200 or 300 rotating anode X-ray generator. For diffractometer scans, a symmetrical transmission technique with a 2θ scanning speed of 1°/min was used. An imaging plate pattern was recorded with the incident beam perpendicular to the film surface. The exposure time was ≤1 min. Diffraction diagrams were reduced from the imaging plate patterns. The decomposition of a pattern into the orthorhombic and hexagonal peaks and amorphous halo was made by assuming a symmetrical function composed of Gaussian and Cauchy profiles, with appropriate proportions for each of the reflections.

The retractive stresses of drawn films were measured during slow heating (0.5 °C/min) and subsequent cooling to room temperature at a constant sample length. For this measurement, a low strain of 0.1% was imposed on the sample at room temperature before heating.

The reactor powder with the higher M_v (5.3×10^6) was used for the X-ray and retractive stress measurements. Its optimum T_d for the second-stage tensile drawing was ∼155 °C.

Results and Discussion

Effect of T_d on Deformation of Reactor Powders. The films of UHMW-PE prepared by compaction of the reactor powder were brittle, with draw not attainable by a straight tensile drawing below the melting point. Above T_m, these films were drawable to only DR ∼ 2 in the molten state. However, these powder films became ductile after having been drawn by solid-state coextrusion at a low EDR of ∼6. Thus, the draw behavior was observed for the second-stage tensile drawing of the initially coextruded samples with an EDR of ∼6.

Figure 1 shows the maximum achieved DR_t ($DR_{t,max}$) as a function of T_d for the second-stage tensile drawing of two UHMW-PE reactor powders having M_v's of 1.8 (part A) and 5.3×10^6 (part B). The data on straight tensile drawing of the UHMW-PE gel (part C), reported by Lemstra et al.,[6] are also included for comparison. For the reactor powders, the ductility increased steadily with T_d, and a $DR_{t,max}$ of 80 was achieved for both the low and high M_v samples at T_d of 145 and 155 °C, respectively. It is noted that even at such high T_d's the draw was effective in terms of MDR, as shown by the steady increase in the tensile properties with DR_t. The maximum tensile moduli and strength achieved at $DR_{t,max}$ of 80 were 110 and 2.0 GPa for the higher M_v reactor powder and 110 and 1.5 GPa for the lower M_v sample, respectively.[4] Above the optimum T_d's, the drawability decreased rapidly due to melting, as shown in Figure 1. The optimum T_d's for the second-stage tensile drawing of these reactor powders were significantly higher than their static T_m (∼140 °C). Such a specific T_d was sensitive to the characteristics of a sample, including M_v. Indeed, the extrudate of a higher M_v exhibited the highest ductility at 155 °C, which is

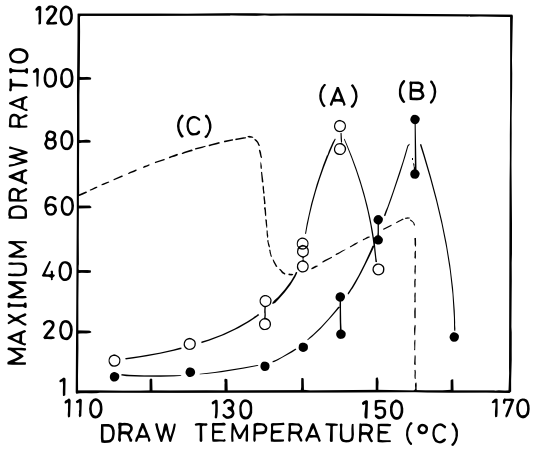

Figure 1. Maximum achieved total draw ratio vs temperature for the two-state drawing of UHMW-PE reactor powders with different M_v's of 1.8×10^6 (A) and 5.3×10^6 (B) and polymerized at 40 °C using a high-activity Ziegler catalyst. The data reported by Lemstra et al.[6] for the UHMW-PE gel (C) are also included for comparison.

15 °C above the DSC melting temperature measured at a heating rate of 5 °C/min without constraint. In contrast, the extrudate of a lower M_v melted, and draw was not attainable at >150 °C.

For straight tensile drawing of the UHMW-PE gel (Figure 1C), $DR_{t,max}$ increased with T_d[6,16,17] and dropped sharply at 135 °C due to melting.[6] At yet higher T_d's, drawability again increased slowly up to 155 °C. Above this temperature drawability was lost. It was noted that the tensile properties achieved in the higher temperature range of 135−155 °C were remarkably low compared to those achieved at T_d < 135 °C. Thus, it was concluded that effective draw in terms of MDR was possible only in a solid state at T_d < 135 °C, whereas at yet higher T_d's draw started from the melt and was not effective.[6] In contrast to the gel, the drawability of the reactor powder with a higher M_v increased steadily with T_d up to 155 °C (Figure 1B). Further, it is interesting to note that the $DR_{t,max}$ and the tensile properties achieved at T_d = 145−155 °C were remarkably high for the reactor powder[4] compared to those achieved for the gel[6] and melt-crystallized sheets;[12] $DR_{t,max}$ of 80 vs 18−60, tensile modulus of 100 vs 4−25 GPa, and strength of 2 vs 0.2−0.5 GPa, respectively, for the reactor powder and for the latter two. These results show that the draw behavior of the reactor powder is significantly different from that of the gel prepared from a semidilute solution and that of a melt-crystallized sheet, reflecting their supermolecular structures.

As stated, tensile drawing of reactor powders was significantly affected by several factors, including polymerization catalyst,[3,18−22] monomer pressure[3] and temperature,[3,18−20] molecular weight,[3,4] and draw technique[1,20,23] and temperature.[4] Figure 2 shows the true stress−strain curves for the second-stage drawing of the higher M_v sample, recorded at 135−160 °C and a constant cross-head speed, giving an initial strain rate of 1 min^{-1}. For drawing at a T_d in the range of 135−150 °C, the draw stress rapidly increased with strain, followed by a fracture. With increasing T_d, the draw stress gradually decreased and the $DR_{t,max}$ increased up to T_d = 155 °C. At a yet higher T_d of 160 °C, the draw stress decreased suddenly to a low level of ∼10 MPa, and the $DR_{t,max}$ also decreased to ∼20. No effective draw was possible at the highest T_d of 160 °C.

X-ray Diffraction and Retractive Stress at Constant Sample Length. To clarify the deformation

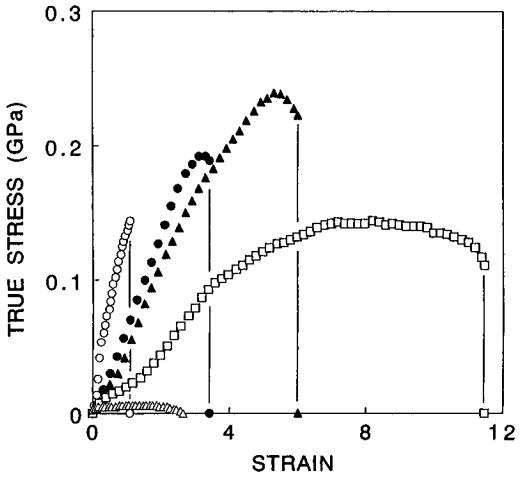

Figure 2. Effect of draw temperature on the true stress–strain curves for the second-stage tensile drawing of an extrusion-drawn film with an EDR = 6.5, prepared from the higher M_v sample. The curves were recorded at 135 (○), 145 (●), 150 (▲), 155 (□), and 160 °C (△).

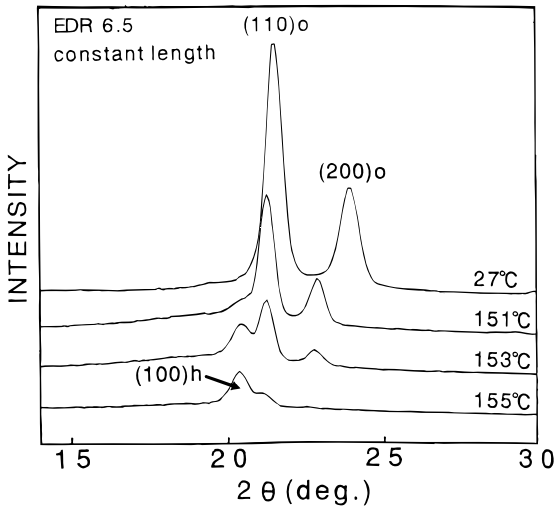

Figure 3. Changes in the WAXD pattern upon heating of an extrusion-drawn sample with EDR = 6.5 kept at a constant length.

mechanism for the second-stage tensile drawing at elevated T_d's, the changes in WAXD pattern and retractive stress were measured as a function of temperature while keeping the sample ends fixed. X-ray equatorial scans were made by using a fiber specimen holder equipped with a temperature controller. Figure 3 shows the variation in the WAXD pattern with temperature for an extrudate with EDR = 6.5, recorded upon heating at a constant length. The hexagonal $(100)_h$ reflection peak appeared at $2\theta = 20.5°$ around 150 °C, and its intensity, as well as that of the amorphous halo, increased upon further heating. At 155 °C, the hexagonal $(100)_h$ reflection and the amorphous halo became predominant, and the orthorhombic $(110)_o$ and $(200)_o$ reflections almost disappeared. Although this extrudate could be drawn at 160 °C, the WAXD pattern at a constant length could not be obtained at this temperature, since the retractive stress relaxed rapidly and the sample was broken due to melting during the X-ray measurement. These results show that an EDR = 6.5 extrudate undergoes crystal/crystal transformation from the orthorhombic to the hexagonal form, combined with partial melting above 150 °C upon heating at a constant length.

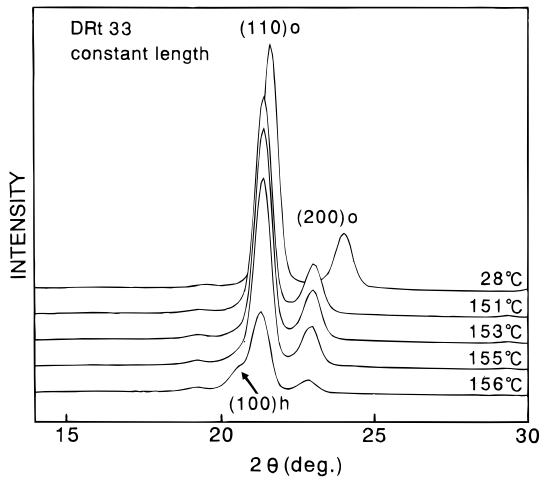

Figure 4. Changes in the WAXD pattern upon heating of a $DR_t = 33$ film kept at a constant length.

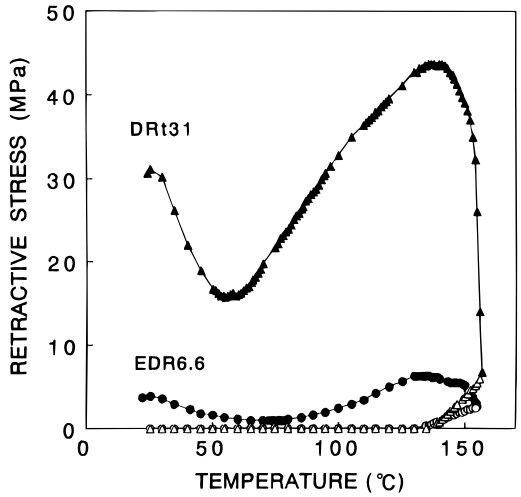

Figure 5. Temperature dependence of the retractive stress along the fiber axis for slow heating (●, ▲) and cooling (○, △) of an extrusion-drawn sample with EDR = 6.5 (circles) and a $DR_t = 31$ film (triangles), both kept at a constant length. The heating and cooling rates were 0.5 °C/min.

When a film with a higher DR_t of 33 was heated at a constant length, the hexagonal $(100)_h$ reflection appeared at a significantly higher temperature of 156 °C, as shown in Figure 4. This sample was broken at 158 °C due to melting. These observations indicate that the transformation from the orthorhombic to the hexagonal form occurs at a higher temperature for a sample with higher DR_t. This is attributed to higher retractive stress at elevated temperatures for the sample with a higher DR_t, as discussed in the following.

Figure 5 shows the temperature dependence of the retractive stress along the fiber axis for two samples with EDR = 6.5 and $DR_t = 31$, recorded during slow heating and cooling. To keep the samples taut, a strain of 0.1% was imposed at room temperature, and then they were heated at ~0.5 °C/min, keeping the sample length constant. The maximum measurement temperature was limited to ~155 °C for the EDR = 6.5 extrudate and 157 °C for the $DR_t = 31$ film. The general features of the retractive stresses with temperature were similar for each of the DRs, both on heating and cooling. Upon heating, the stress steadily decreased due to relaxation and reached a minimum at 60–75 °C. Subsequently, it increased significantly up to ~135 °C, which is likely due to the entropic force associated with

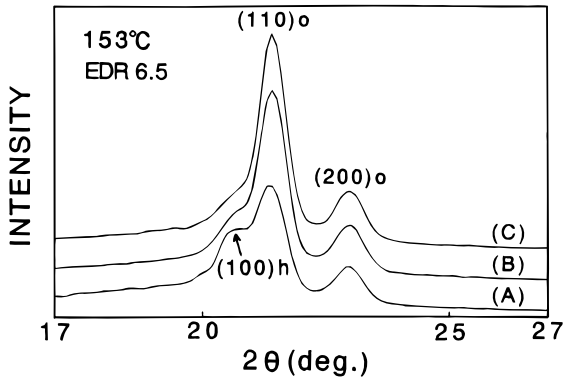

Figure 6. WAXD patterns observed at 153 °C for an extrusion-drawn sample with EDR = 6.5 kept at a constant length (A), subsequently loaded with a load of 12 MPa (B), and measured 10 min after the scan (B) was finished (C).

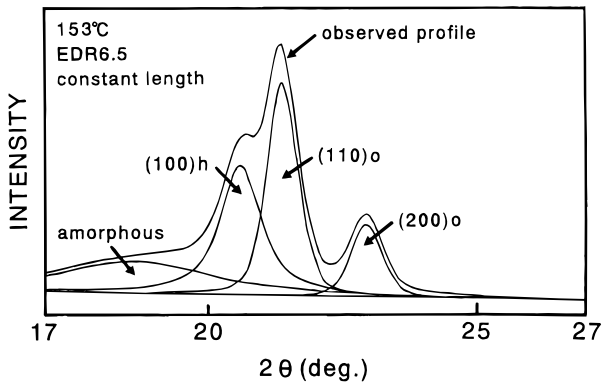

Figure 7. Decomposition of the pattern of panel A into the orthorhombic and hexagonal reflection peaks and the amorphous halo.

the molecular motion in amorphous regions and the onset on the motion within crystals (α-relaxation).[24] At yet higher temperatures, it decreased slowly at 140−150 °C and then rapidly at 150−155 °C, where the transformation from the orthorhombic to the hexagonal phase occurred (Figures 3 and 4) and the chains easily slid past each other. Upon cooling, the retractive stress relaxed with decreasing temperature and reached ∼0 at 130−135 °C. Upon further cooling down to room temperature, the samples became loose due to the negative thermal expansion of the oriented polyethylene.[25] The retractive stress observed upon a heating process was considerably higher for the sample with a higher DR_t throughout the temperatures. The fact that the crystal transformation from the orthorhombic to the hexagonal form occurred at a higher temperature for the sample with a higher DR_t (150 °C for EDR = 6.5 vs 156 °C for DR_t = 31 in Figures 3 and 4) is related to the higher retractive stress for the sample with higher DR, as will be discussed in the following.

Effect of Tensile Load on X-ray Diffraction Pattern. Figure 6 shows a series of WAXD equatorial patterns for the extrudate heated at 153 °C with the sample ends fixed (part A), followed by tensile loading of 12 MPa (part B). The third scan (part C) was made 10 min after the second scan. The resolution of the pattern in Figure 6A into the orthorhombic and hexagonal reflection peaks and the amorphous halo was made by assuming a symmetrical function consisting of Gaussian and Cauchy profiles for each of the peaks, as shown in Figure 7. The peak position in 2θ and the proportion of Gaussian and Cauchy profiles for the amorphous halo used for the pattern decomposition

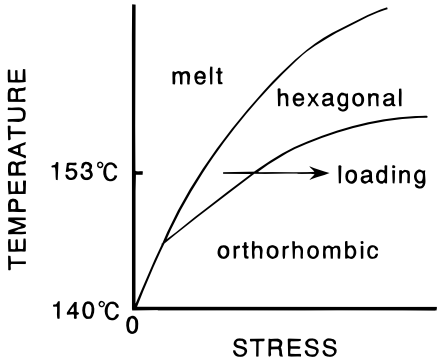

Figure 8. Stress−temperature phase diagram for a drawn UHMW-PE reactor powder film. The arrow represents the process of the deformation after loading at 153 °C for an EDR = 6.5 extrudate (Figure 7).

were determined from the profile observed on the melt at 160 °C for the melt-crystallized film of the same UHMW-PE. The hexagonal $(100)_h$ reflection peak is clearly resolved at $2\theta = 20.6°$ in Figure 7. When a tensile load of 12 MPa was imposed on the sample (Figure 6B), the intensity of the initial hexagonal $(100)_h$ reflection (Figure 6A) quickly decreased and the orthorhombic $(110)_o$ and $(200)_o$ reflection peaks intensified (Figure 6B). Such a change occurred instantly upon load application, and no significant change was found in the pattern recorded after 10 min (Figure 6C). These observations have an important implication on the morphology drawn only to a low EDR of 6.5. The coexistence of the orthorhombic, hexagonal, and amorphous phases at 153 °C indicates that the applied stress was not distributed homogeneously within the drawn sample, i.e., the crystals under a sufficient tension remained the orthorhombic crystals, those under an intermediate tension transformed into the hexagonal form, and the others under less tension melted.

The temperature−stress phase diagram for such behavior is similar to that reported for the temperature−pressure phase diagram[26] and is represented schematically in Figure 8. The hexagonal crystals at 153 °C and at a constant sample length (Figure 6A), which is represented by the starting point of the arrow in Figure 8, transform into the orthorhombic form upon loading. After loading, the sample elongated slowly and, thus, the stress increased gradually.

Real-Time X-ray Diffraction Pattern during Sample Drawing. The preceding results, consistent with a previous report,[27] indicate that both the orthorhombic and the hexagonal phases are thermally stabilized by the application of an external stress along the fiber axis. Thus, to determine the real phase structures and the morphological changes during the second-stage drawing of the extrudate at T_d's above the static melting point of PE, real-time X-ray measurements were made by using imaging plates combined with a high-temperature drawing device.[15] At a constant draw rate, the strain rate decreased gradually as the sample was elongated. Thus, the initial strain rates were adjusted to 0.2−0.7 min^{-1} for the DR_t of samples, so as to give the same elongation rate as each sample passed through any DR_t.

Figure 9 shows a series of imaging plate patterns recorded during the drawing of an extrudate with EDR = 6.5 at a T_d of 150 °C. Before drawing, the sample showed the orthorhombic $(110)_o$ and $(200)_o$ reflection arcs on the equator and a uniform ring of the amorphous halo (Figure 9A). In addition, a weak hexagonal $(100)_h$

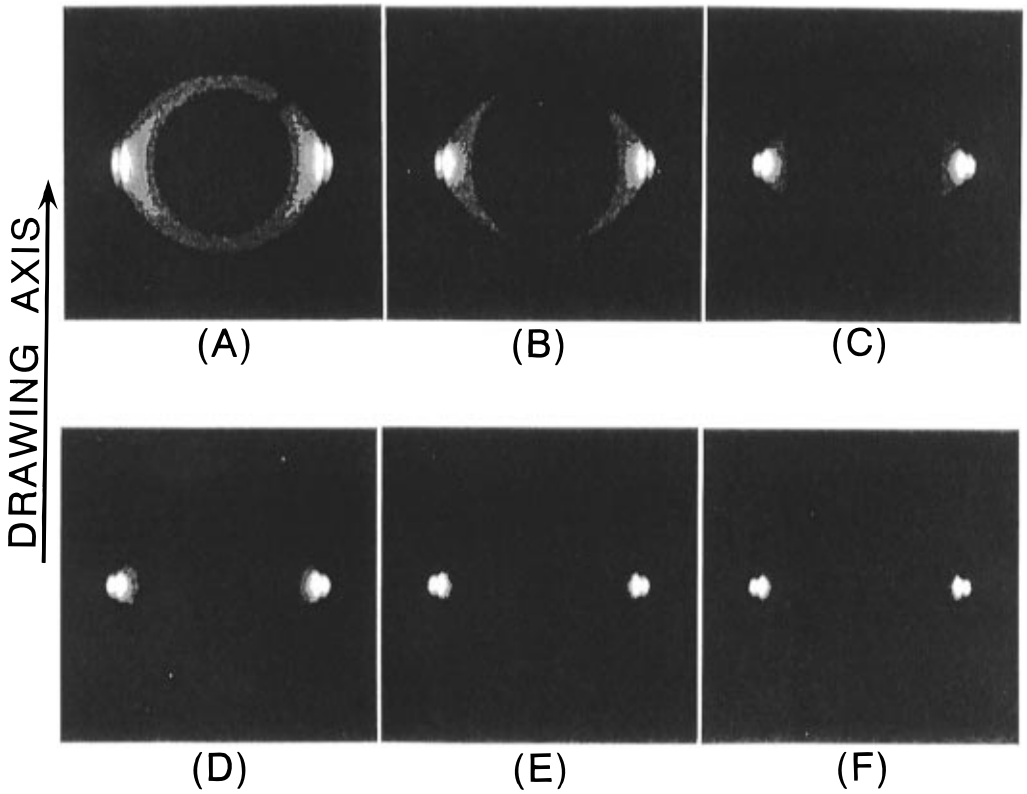

Figure 9. Imaging plate patterns observed during drawing of an extrudate with EDR = 6.5 at 155 °C: (A) before drawing and (B) at DR*t* = 6.5−11, (C) 11−16, (D) 16−20, (E) 20−25, and (F) 25−29. The DR_t ranges were estimated from the draw rates and the X-ray exposure time.

reflection appeared between the amorphous halo and the $(110)_o$ reflection. The azimuthal intensity distribution of the $(100)_h$ arc is significantly broad compared to those of the orthorhombic reflections, indicating that the hexagonal crystals were less oriented than the orthorhombic crystals. Thus, less stress was imposed on the hexagonal crystals, consistent with the preceding finding that a higher stress stabilizes the orthorhombic form. When draw was initiated, the amorphous halo rapidly decreased in intensity and concentrated on the equator. The $(110)_o$ and $(200)_o$ reflection arcs transformed to sharp spots at higher DR_t's, showing a rapid increase in the chain orientation with DR_t. Further, the weak hexagonal $(100)_h$ reflection existed before drawing disappeared and immediately when draw was initiated.

Although the imaging plate patterns gave important information on the orientation of the two crystal forms and the amorphous component, they were not sensitive to the change in intensities of these reflections upon drawing. Thus, the diffraction diagrams on the equator in Figure 9 were reduced and are shown in Figure 10. Before drawing (Figure 10A), the orthorhombic $(110)_o$ and $(200)_o$ reflections overlapped with the amorphous halo were predominant. In addition, a weak hexagonal $(100)_h$ reflection appeared as a low-angle shoulder of the $(110)_o$ reflection. These features are consistent with the observation by the WAXD scan for the extrudate kept at a constant length and ~150 °C (Figure 3).

On the equatorial scan in Figure 10A, the hexagonal $(100)_h$ peak is not clearly seen. As the azimuthal intensity distribution of the hexagonal reflection was broader than those of the orthorhombic peaks, the diffraction diagram at an angle of 10° to the equator was reduced, as shown in Figure 11. Each of the crystalline peaks and the amorphous halo are well resolved, and the $(100)_h$ reflection is clearly seen at 2θ = 20.6°. Note that the intensity ratio of the $(100)_h$ to the $(110)_o$ reflection is higher for the pattern measured 10° from the equator (Figure 11) than for that on the equator (Figure 10A). This clearly shows that the chain orientation along the fiber axis is significantly lower for the hexagonal crystalline form than for the orthorhombic crystals.

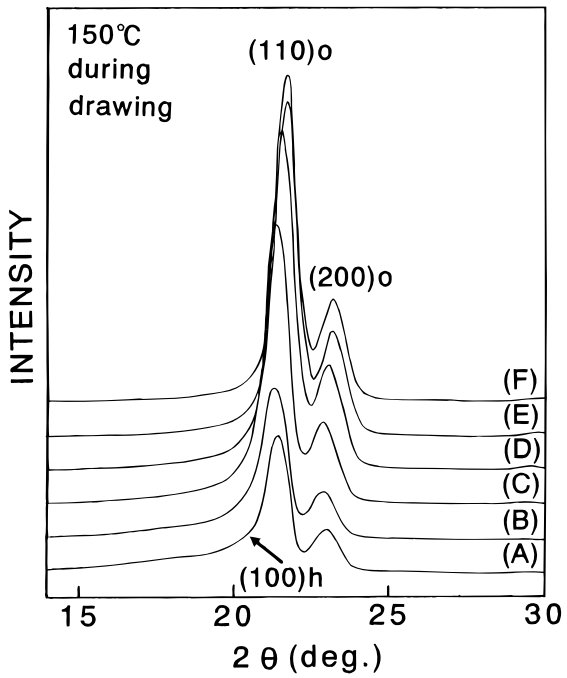

Figure 10. Line profiles on the equator reduced from the imaging plate patterns in Figure 9: (A) EDR = 6.5 and (B) DR_t = 6.5−11, (C) 11−16, (D) 16−20, (E) 20−25, and (F) 25−29.

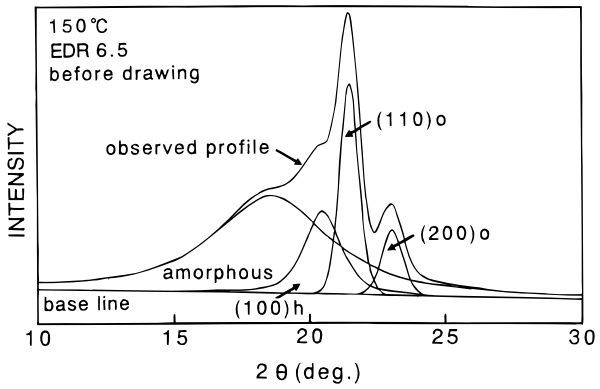

Figure 11. Diffraction diagram reduced along the line inclined at +10° from the equator of the imaging plate pattern in Figure 9A.

Upon drawing of an extrudate with EDR = 6.5 at 150 °C, the intensity of the amorphous halo having a maximum at $2\theta = 19.6°$ decreased rapidly, and those of the orthorhombic reflections increased with DR_t, indicating that the stress-induced crystallization occurred rapidly. Even at an early stage of drawing, the initially weak hexagonal $(100)_h$ reflection disappeared at a small elongation. These results show that the major deformation proceeded in a highly crystalline state during drawing at 150 °C, which is ~10 °C above the T_m of PE.

Figure 12 shows a series of imaging plate patterns recorded during drawing of an extrudate with EDR = 6.5 at a higher T_d of 155 °C. This was the optimum T_d, allowing the highest DR_t and the highest tensile properties to be achieved for the higher M_v sample. Before drawing (Figure 12A), the hexagonal $(100)_h$ reflection and a uniform amorphous ring were predominant, and the weak orthorhombic reflections were also observed. The patterns of this extrudate recorded at 150 and 155 °C (Figures 9A and 12A) before drawing show that the chain orientation in the crystalline regions is significantly higher at the higher temperature. This is because the crystals well oriented along the draw direction receive a significant retractive stress and are stabilized, whereas those less oriented melted since they received a lower stress. When draw was initiated, the amorphous halo gradually concentrated on the equator and its intensity decreased, indicating that the stress-induced orientation in the amorphous regions with crystallization proceeded steadily during drawing at 155 °C.

X-ray diffraction patterns on the equator during drawing at 155 °C were reduced from Figure 12 and are shown in Figure 13. The pattern before drawing (Figure 13A) shows a strong $(100)_h$ hexagonal reflection, weak orthorhombic reflections, and a broad amorphous halo. This pattern is comparable to that observed by a diffractometer scan at a constant sample length at 155 °C (Figure 3). Upon drawing, the intensity of both the hexagonal $(100)_h$ reflection and the amorphous halo decreased gradually, and those of the orthorhombic reflections rapidly increased with increasing DR_t. At a higher DR_t of 16−20, the hexagonal reflection disappeared. These observations indicate that the stress- and orientation-induced crystallization and the crystal/crystal transformation from the hexagonal to the orthorhombic form proceeded during drawing, even at a high T_d of 155 °C. Thus, the deformation proceeded in a highly crystalline state where the orthorhombic phase is predominant, during the second-stage drawing of an EDR = 6.5 extrudate even at 155 °C, and resulted in an efficient draw as evaluated by tensile properties vs DR_t.[4]

Figure 14 shows the changes in the imaging plate pattern during drawing from the initial DR_t of 22 to 38

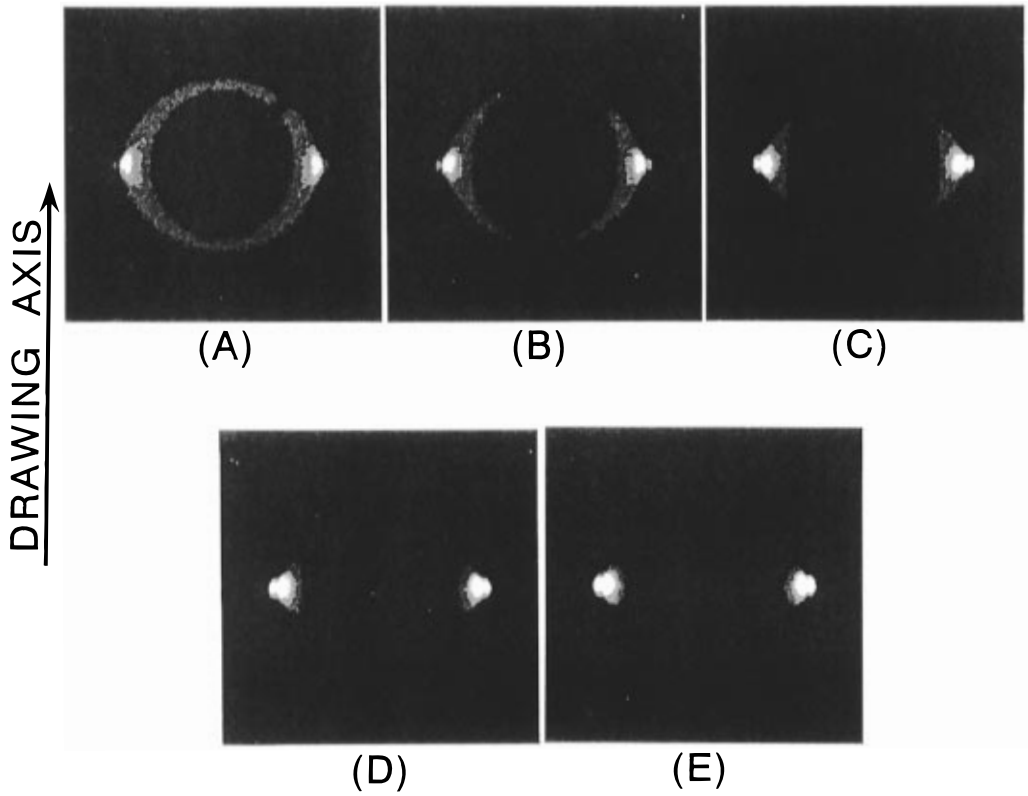

Figure 12. Imaging plate patterns observed during drawing of an EDR = 6.5 extrudate at 155 °C: (A) before drawing and (B) DR*t* = 6.5−10, (C) 10−13, (D) 13−16, and (E) 16−20.

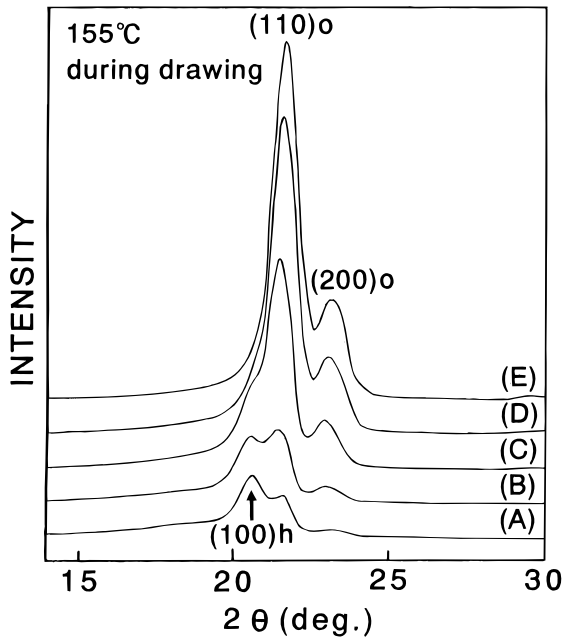

Figure 13. Line profiles on the equator reduced from the imaging plate patterns in Figure 12: (A) EDR = 6.5 and (B) DR_t = 6.5−10, (C) 10−13, (D) 13−16, and (E) 16−20.

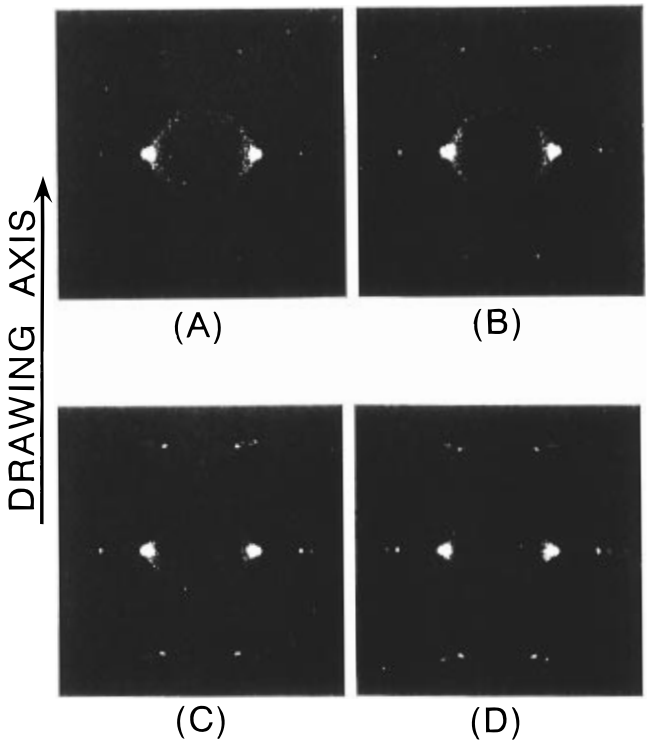

Figure 14. Series of imaging plate patterns observed during drawing of a film with an initial DR_t of 22 at 156−160 °C: (A) before drawing at 156 °C; (B) DR_t = 22−25 at 156 °C; (C) DR_t = 28−32 at 156 °C; and (D) DR_t = 35−38 at 160 °C.

at yet higher T_d's of 156−160 °C. The line profiles on the equator of these patterns are shown in Figure 15. Before drawing at 156 °C, a weak hexagonal $(100)_h$ peak and amorphous halo were clearly observed (Figure 15A). As has been observed for the drawing of a lower EDR sample at lower T_d's, the intensity of these peaks decreased gradually and those of the orthorhombic reflections increased rapidly upon elongation. Even when the T_d was raised to 160 °C during drawing, the hexagonal phase was barely evident, with no significant increase in the amorphous halo and with the orthorhombic phase predominant. Of further note is that the intensity of the amorphous halo was weak, showing high crystallinity during drawing at 156−160 °C.

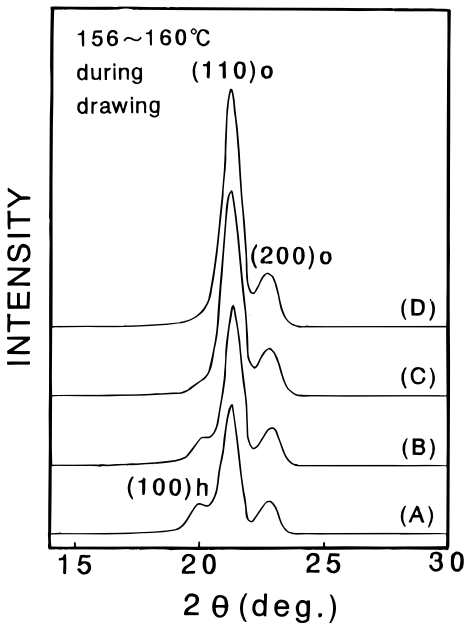

Figure 15. Line profiles on the equator reduced from the imaging plant patterns in Figure 14: (A) DR_t = 22 at 156 °C, (B) 22−25 at 156 °C, (C) 28−32 at 156 °C, and (D) 35−38 at 160 °C.

These results show that the initially hexagonal phase and unoriented amorphous component, observed before drawing at high T_d's, transformed into the highly oriented orthorhombic phase during drawing. These facts indicate that the major mechanism for deformation at T_d's of 155−160 °C is plastic deformation in a crystalline state, where the orthorhombic form is predominant. Such a deformation is likely related to the specific structure of the UHMW-PE reactor powder, the existence of a network structure, including intercrystalline tie molecules, and the entanglement network, which effectively transmit the applied stress within a sample.

Conclusions

UHMW-PE reactor powders, extrusion drawn to a low EDR of ∼6 (first-stage draw), were drawn by tensile force (second-stage draw). The optimum T_d for the second-stage drawing of the extrudates was often above the static T_m of PE, depending on the characteristics of the samples. This is markedly different from the drawing behavior of the UHMW-PE gel. The WAXD patterns measured upon heating of the extrusion-drawn samples, kept at a constant length, showed that a part of the initially orthorhombic crystals transformed to the hexagonal and amorphous phases above 150 °C. Upon further heating, the transformation proceeded further. The chain orientation along the fiber axis was lower for the hexagonal phase than for the orthorhombic. The coexistence of the three phases at elevated temperatures under sample tension is ascribed to the inhomogeneous stress distribution within a drawn sample. With increasing sample DR_t, the crystal/crystal transformation and partial melting occurred at higher temperatures, corresponding to an increase in the retractive stress with increasing DR_t. The phase structure at elevated temperatures was affected considerably by the stress applied along the fiber axis. When draw was initiated

at 150−155 °C, the initially hexagonal phase rapidly transformed into the orthorhombic form and the amorphous component also crystallized into the orthorhombic, since the stress and amorphous chain orientation increased during draw. Even when the temperature was raised to 160 °C during drawing the orthorhombic phase was predominant, with no hexagonal phase evident and no significant increase in the amorphous phase. Thus, the deformation in the second-stage drawing of compacted reactor powder films proceeded in a highly crystalline state where the orthorhombic form was predominant, at least up to 160 °C, which is significantly above the static T_m of UHMW-PE of ~140 °C. Such a draw was effective in terms of MDR, resulting in high tensile properties of the drawn products.

References and Notes

(1) Kanamoto, T.; Ohama, T.; Tanaka, K.; Takeda, M.; Porter, R. S. *Polymer* **1987**, *28*, 1617.
(2) Ohama, T.; Kanamoto, T.; Tanaka, K.; Takeda, M.; Porter, R. S. *Rep. Prog. Polym. Phys. Japan* **1987**, *30*, 333.
(3) Sano, A.; Matsuura, K.; Kanamoto, T. Manuscript in preparation.
(4) Watanabe, M.; Mizorogi, K.; Uehara, H.; Kanamoto, T.; Sano, A.; Matsuura, K. *Rep. Prog. Polym. Phys. Japan* **1993**, *36*, 285.
(5) Pennings, A. J.; Zwijnenburg, A. *J. Polym. Sci., Polym. Phys. Ed.* **1979**, *17*, 1011.
(6) Lemstra, P. J.; Van Aerle, N. A. J. M.; Bastiaansen, C. W. M. *Polym. J.* **1987**, *19*, 85.
(7) Van Aerle, N. A. J. M.; Lemstra, P. J.; Braam, A. W. M. *Polym. Commun.* **1989**, *30*, 7.
(8) Wunderlich, B.; Arakawa, T. *J. Polym. Sci. Part A* **1964**, *2*, 3697.
(9) Yasuniwa, M.; Nakafuku, C.; Takemura, T. *Polym. J.* **1973**, *4*, 526.
(10) Tanaka, H.; Takemura, T. *Polym. J.* **1980**, *12*, 355.
(11) Yamamoto, T.; Miyaji, H.; Asai, K. *Jpn. J. Appl. Phys.* **1977**, *16*, 1891.
(12) Kaito, A.; Nakayama, K.; Kanetsuna, H. *Polym. J.* **1982**, *14*, 757.
(13) Porter, R. S.; Wang, L. H. *J. Macromol. Chem. Phys.* **1995**, *C* (35), 63.
(14) Van Aerle, N. A. J. M.; Lemstra, P. J.; Kanamoto, T.; Bastiaansen, C. W. M. *Polymer* **1991**, *32*, 34.
(15) Murakami, S.; Tanno, K.; Tsuji, M.; Kohjiya, S. *Bull. Inst. Chem. Res. Kyoto Univ.* **1995**, *72*, 418.
(16) Sawatari, C.; Matsuo, M. *Colloid Polym. Sci.* **1985**, *263*, 783.
(17) Anandakumaran, K.; Roy, S. K.; Manley, R. St. J. *Macromolecules* **1988**, *21*, 1746.
(18) Smith, P.; Chanzy, H. D.; Rozinger, B. P. *Polym. Commun.* **1985**, *26*, 258.
(19) Smith, P.; Chanzy, H. D.; Rotzinger, B. P. *J. Mater. Sci.* **1987**, *22*, 523.
(20) Pawlikowski, G. T.; Mitchell, D. J.; Porter, R. S. *J. Polym. Sci., Polym. Phys. Ed.* **1988**, *26*, 1865.
(21) Wang, L. H.; Ottani, S.; Porter, R. S. *Polymer* **1991**, *32*, 1774.
(22) Selikhova, V. I.; Zubov, Yu. A.; Sinevich, E. A.; Chvalun, S. N.; Ivancheva, N. I.; Smol'yanova, O. V.; Ivanchev, S. S.; Bakeev, N. F. *Polym. Sci. USSR* **1992**, *34*, 151.
(23) Zachariades, A. E.; Watts, M. P. C.; Kanamoto, T.; Porter, R. S. *J. Polym. Sci., Lett. Ed.* **1978**, *17*, 487.
(24) Kajiyama, T.; Okada, T.; Sakoda, A.; Takayanagi, M. *J. Macromol. Sci.-Phys.* **1974**, *B* (7), 583.
(25) Capiati, N. J.; Porter, R. S. *J. Polym. Sci., Polym. Phys. Ed.* **1977**, *15*, 1427.
(26) Leute, U.; Dillbopf, W. *Collid Polym. Sci.* **1980**, *258*, 354.
(27) Rastogi, S.; Odell, J. A. *Polym. Commun.* **1993**, *34*, 523.

MA951222Y